Available online at www.sciencedirect.com
SCIENCE DIRECT
International Journal of Thermal Sciences 45 (2006) 390–404
International Journal of Thermal Sciences
www.elsevier.com/locate/ijts

Numerical investigation on laminar forced convection and entropy generation in a curved rectangular duct with longitudinal ribs mounted on heated wall

T.H. Ko *

Department of Mechanical Engineering, Lunghwa University of Science and Technology, 300, Wan-Shou Rd. Sec. 1, Kueishan, 33306 Taoyuan, Taiwan, ROC

Received 12 April 2005; received in revised form 9 June 2005; accepted 9 June 2005

Available online 1 August 2005

Abstract

Three-dimensional laminar forced convective flow and entropy generation in a 180-deg curved rectangular duct with longitudinal ribs equipped on the heated wall are investigated by numerical methods. The development of secondary vortices, temperature and local entropy generation distributions as well as the overall entropy generation in whole flow fields, including the entrance and fully developed region, are analyzed. The effects of rib size are particularly highlighted in the present paper. Calculations of cases with various rib sizes under different Dean numbers and external heat fluxes are carried out to examine the influence of rib on the flow field and entropy generation. The entropy generated from frictional irreversibility and heat transfer irreversibility is investigated separately in detail. The results reveal that the addition of rib can effectively reduce the entropy generation from heat transfer irreversibility since the secondary vortices are augmented by the rib, through which the heat transfer performance is enhanced, in turn making the temperature gradient become smoother. Nevertheless, the entropy generation due to frictional irreversibility is raised at the same time because larger fluid friction is resulted from the wider solid walls and the complex flows disturbed by ribs. Due to the opposite influences of rib on the entropy generations from irreversibilities, the analysis of the optimal trade-off is carried out based on the minimal entropy generation principle. The optimal rib size which induces the minimal entropy generation in the flow fields is found to be dependent on the external heat flux and Dean number. Even under some flow conditions, the resultant entropy generation could not be reduced but becomes worse when ribs are added. These results provide worthwhile information for considerations of adding ribs on a curved duct and the determinations of rib sizes from view point of thermodynamic second law.

Keywords: Curved rectangular duct; Forced convection; Irreversibility; Entropy generation; CFD

1. Introduction

The study of heat transfer and flows through a curved duct is of fundamental importance for industrial applications such as turbomachinery, refrigeration and air conditioning systems, heat exchangers, and the blade-to-blade passage for cooling system in modern gas turbines. The principal flow feature in curved ducts is the presence of secondary flow motion generated as a result of curvature effects and centrifugal force. The secondary vortices promote fluid mixing, and in turn enhance the heat transfer performance. However, they result in more serious pressure drop in the flow passage. During past several decades, the flow dynamics and heat transfer in curved ducts with various cross-sectional shapes, including circular, rectangular and elliptic, have received continuous attention [1–8]. Because of the practical importance, many studies focus on the flows in curved ducts with rectangular cross-sections. The flow field in a fully developed laminar flow in a curved rectangular channel was analyzed by Cheng et al. [3], in which the influence of the aspect ratio on the Dean vortices and secondary-flow instability was emphasized. The flow structure in a helical

* Tel.: +886 2 82093211; fax: +886 2 82091475.
E-mail address: thko@mail.lhu.edu.tw (T.H. Ko).

1290-0729/$ – see front matter
doi:10.1016/j.ijthermalsci.2005.06.005

Nomenclature

a	width of the cross-sectional area of rectangular curved duct ..... m	Re	Reynolds number
b	height of the cross-sectional area of rectangular curved duct ..... m	r_c	radius of curvature ..... m
Be	Bejan number	S'''_P	volumetric entropy generation rate due to friction ..... $W\cdot m^{-3}\cdot K^{-1}$
d_e	hydraulic diameter ..... m	S'''_T	volumetric entropy generation rate due to heat transfer ..... $W\cdot m^{-3}\cdot K^{-1}$
De	Dean number, $= Re(d_e/r_c)^{1/2}$	S'''_{gen}	total volumetric entropy generation rate ..... $W\cdot m^{-3}\cdot K^{-1}$
h	rib height ..... m	S^*_P	non-dimensional entropy generation rate due to friction
$\bar{h}$	average heat transfer coefficient in the rectangular curved duct ..... $W\cdot m^{-2}\cdot K^{-1}$	S^*_T	non-dimensional entropy generation rate due to heat transfer
k	thermal conductivity of fluid .... $W\cdot m^{-1}\cdot K^{-1}$	S^*_{gen}	non-dimensional entropy generation rate
k_s	thermal conductivity of steel .... $W\cdot m^{-1}\cdot K^{-1}$	T	temperature ..... K
Nu	Nusselt number, $= \bar{h}d_e/k$	T_0	temperature at duct entrance ..... K
P	pressure ..... Pa	V	average velocity in duct ..... $m\cdot s^{-1}$
q''	wall heat flux ..... $W\cdot m^{-2}$	μ	molecular viscosity ..... $kg\cdot m^{-1}\cdot s^{-1}$
q^*	non-dimensional heat flux	ρ	density ..... $kg\cdot m^{-3}$
$\dot{Q}$	heat transfer rate ..... W		
R	gas constant ..... $J\cdot kg^{-1}\cdot K^{-1}$		

rectangular duct and the effects of curvature and torsion in the flow were investigated by Bolinder [4]. In the study of Wang [5], the buoyancy-force-driven transition and its effects on the heat transfer in a rotating curved rectangular channel were studied. Through the numerical investigations on the fully developed laminar forced convection in curved rectangular and elliptic ducts carried out by Silva et al. [6], a general correlation of Nusselt number and friction factor as a function of Dean number (De) and the cross-sectional aspect ratio of the duct was proposed. The secondary flow and convective heat transfer in curved rectangular ducts with external heating were investigated by Chandratilleke [7] using experimental method, and Chandratilleke and Nursubyakto [8] using both of numerical and experimental methods. In their studies, the effects of Dean number and duct aspect ratio on the heat transfer coefficient and flow fields were analyzed. For enhancing the heat transfer performance, Camci and Rizzo [9] added a fence on the heated wall of a 90-deg turning rectangular curved duct. Through their experimental study, they found the added fence could effectively raise the heat transfer performance of the turbulent convection in the curved duct.

The primary concern of the heat exchanger design is twofold: the effective heat transfer performance and the least pressure drop. However, an embarrassing situation exits in the practical design work, i.e. a design parameter adjusted to enhance heat transfer performance inevitably accompanies an increase of pressure drop. The conflict situation challenges the design work. The optimal trade-off by selecting the most appropriate configuration and the best flow conditions becomes critical and unavoidable. For determining the optimal design, the minimal entropy generation principle has been widely adopted to evaluate a thermal system [10,11]. The entropy generation in a heat transfer process may be resulted from heat transfer irreversibility or fluid frictional irreversibility. An adjustment of design parameters would cause opposing contributions to irreversibilities. The systematic methodology of computing entropy generation through heat and fluid flow in several heat exchangers has been described by Bejan [10,11]. Based on the minimal entropy generation principle, optimal designs of thermal systems have been widely proposed from the viewpoint of thermodynamic Second Law [10–17]. Several examples are as follows: the optimization work for convective heat transfer through a duct with constant heat flux by Nag and Kumar [12]; the irreversibility analysis in various duct geometries with constant wall heat flux by Sahin [13,14]; the optimal analysis of fin geometry in an electronic cooling system based on the exergoeconomic by Shuja [15]; the optimal analysis of rectangular channels with square pin-fins by Sara et al. [16]; and the optimizing work for the laminar forced convection in helical coils by Ko and Ting [17]. In view of that most of the previous investigations on convective flows in curved rectangular ducts are restricted to the analysis based on thermodynamic First Law, a recent work of Ko and Ting [18] investigated the entropy generation due to laminar forced convection in a curved rectangular duct with constant wall heat flux. In the study, the influence of external heat flux, Dean number and cross-sectional aspect ratio on the entropy generation were emphasized, through which the optimal Dean number and aspect ratio according to relevant design parameters to induce the minimal entropy generation and least irreversibility were reported. According to a recent research of Camci and Rizzo [9], the fence mounted on the heated wall of a rectangular curved duct could effectively raise the heat transfer performance. However, since their study was restricted

to the thermodynamic First Law, the current study is motivated. The present paper intends to investigate the laminar forced convection and entropy generation in a curved rectangular duct with longitudinal ribs mounted on the heated wall with numerical methods. The effects of the rib on the flow features and entropy generation are the principal concerns. Through the entropy generation analysis and minimal entropy generation principle, the optimal rib size in the rectangular curved duct with different flow conditions will be discussed in the paper.

2. Physical model

Fig. 1 shows the semi-circular curved rectangular duct analyzed in the present paper. The curved duct represents a heat exchanger passage. Heat is transferred through the outer wall of the duct, and is transported by the cooling air from duct entrance. A steel rib with square cross-section is mounted at the midway of the heated wall as shown in Fig. 1 for enhancing the heat transfer performance. The cross-section of the curved duct is a square with side length a. The Reynolds number (Re), Nusselt number (Nu) and Dean number (De) for the current problem are defined as follows:

$$Re = \rho V d_e/\mu \tag{1}$$

$$Nu = \bar{h} d_e/k \tag{2}$$

and

$$De = Re(d_e/r_c)^{1/2} \tag{3}$$

where V and $\bar{h}$ are the average velocity and average heat transfer coefficient of the flow in the curved duct; d_e is the characteristic length defined as $4A/P_W$, where A and P_W are the area and wetted perimeter of the square cross-section, respectively; r_c is the curvature radius of the curved duct. The rib height is h; the density and thermal conductivity of the steel rib are 7900 kg·m^{-3} and 48 W·m^{-1}·K^{-1}, respectively. Air has been selected as working fluid in the present study. Since temperature change in the flow field is very small, the thermophysical properties of molecular viscosity (μ) and thermal conductivity (k) are assumed to be constant as 1.846×10^{-5} kg·m^{-1}·s^{-1} and 0.0263 W·m^{-1}·K^{-1}, respectively. The buoyancy force due to gravity has been included in considerations. The gravity direction is indicated in Fig. 1. The fluid density at duct entrance according to the fluid temperature T_0 is 1.161 kg·m^{-3}. The non-dimensional wall heat flux, q^*, is defined according to the external wall heat flux, q'', as

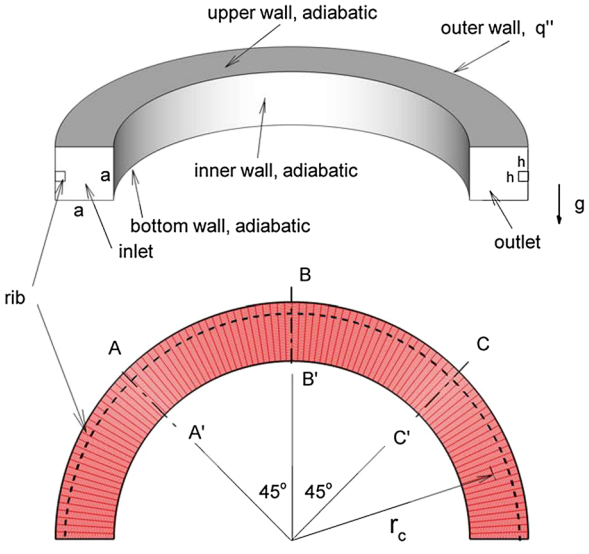

Fig. 1. Geometry and coordinate system of a curved rectangular duct.

$$q^* = q'' d_e/kT_0 \tag{4}$$

In a baseline case of the present study, q^* and De are fixed as 0.112 and 2000, respectively. Except the baseline case, q^* is varied as 0.056, 0.224 and 0.448, while De is varied as 500, 1000 and 3000, to investigate the influence of external heat flux and Dean number on flow fields. For various flow conditions, the calculated cases cover the curved ducts with and without ribs. In the cases with rib, the rib size, h/d_e, is varied as 1/10, 1/7 and 1/5 to investigate its influences.

3. Mathematical model and numerical method

3.1. Mathematical model

The present problem is three-dimensional, laminar and steady. The conjugated heat transfer phenomenon including the convection in fluid flow and the conduction in steel rib are considered simultaneously in the present analysis. For fluid flow, the relevant equations are continuity equation, Navier–Stokes equation, energy equation and equation of state. For steel rib, the heat conduction equation is considered. The equations in tensor form are as follows.

For fluid flows:

$$\frac{\partial(\rho U_i)}{\partial x_i} = 0 \tag{5}$$

$$\frac{\partial}{\partial x_j}(\rho U_j U_i) = -\frac{\partial P}{\partial x_i} + \frac{\partial}{\partial x_j}\left[\mu\left(\frac{\partial U_i}{\partial x_j} + \frac{\partial U_j}{\partial x_i}\right) - \frac{2}{3}\mu\frac{\partial U_k}{\partial x_k}\delta_{ij}\right] + \rho g_i \tag{6}$$

$$\frac{\partial}{\partial x_j}\left(\rho U_j C_p T - k\frac{\partial T}{\partial x_j}\right) = U_j\frac{\partial P}{\partial x_j} + \left[\mu\left(\frac{\partial U_i}{\partial x_j} + \frac{\partial U_j}{\partial x_i}\right) - \frac{2}{3}\mu\frac{\partial U_k}{\partial x_k}\delta_{ij}\right]\frac{\partial U_i}{\partial x_j} \tag{7}$$

$$P = \rho RT \tag{8}$$

For steel rib:

$$\frac{\partial}{\partial x_j}\left(k_s\frac{\partial T}{\partial x_j}\right) = 0 \tag{9}$$

The boundary conditions are specified as follows. The uniform axial velocity is set at duct entrance. At outlet, the diffusion flux in the direction perpendicular to the outlet plane for all velocity components and temperature are set to zero. Non-slip conditions are specified on the duct wall and rib wall. As shown in Fig. 1, the constant heat flux is specified only on the outer wall, whereas on other walls of the curved duct adiabatic condition is applied. At the interface between fluid and rib surface, the energy balance of convection in fluid flow and conduction in steel rib is applied to couple the conjugated heat transfer process.

After the velocity and temperature distributions of the flow field are solved by using Eqs. (5)–(9) and the accompanied boundary conditions, the volumetric entropy generation due to the heat transfer irreversibility (S'''_{T}) and the fluid frictional irreversibility (S'''_{P}) can be calculated by the following equations [11]:

$$S'''_{\mathrm{T}} = \frac{k}{T^2}\left(|\nabla T|\right)^2 \tag{10}$$

$$S'''_{\mathrm{P}} = \frac{\mu}{T}\left(\frac{\partial U_i}{\partial x_j} + \frac{\partial U_j}{\partial x_i}\right)\frac{\partial U_i}{\partial x_j} \tag{11}$$

The total volumetric entropy generation in the flow field can be obtained by

$$S'''_{\mathrm{gen}} = S'''_{\mathrm{T}} + S'''_{\mathrm{P}} \tag{12}$$

Bejan number (*Be*) proposed by Paoletti et al. [19], which describes the contribution of heat transfer entropy on overall entropy generation, is defined as

$$Be = S'''_{\mathrm{T}} / S'''_{\mathrm{gen}} \tag{13}$$

Obviously, the *Be* ranges from 0 to 1; $Be = 0$ and $Be = 1$ are two limiting cases representing the irreversibility is dominated by fluid friction and heat transfer, respectively. When $Be = 0.5$, the entropy generation rates from heat transfer and fluid friction are equal.

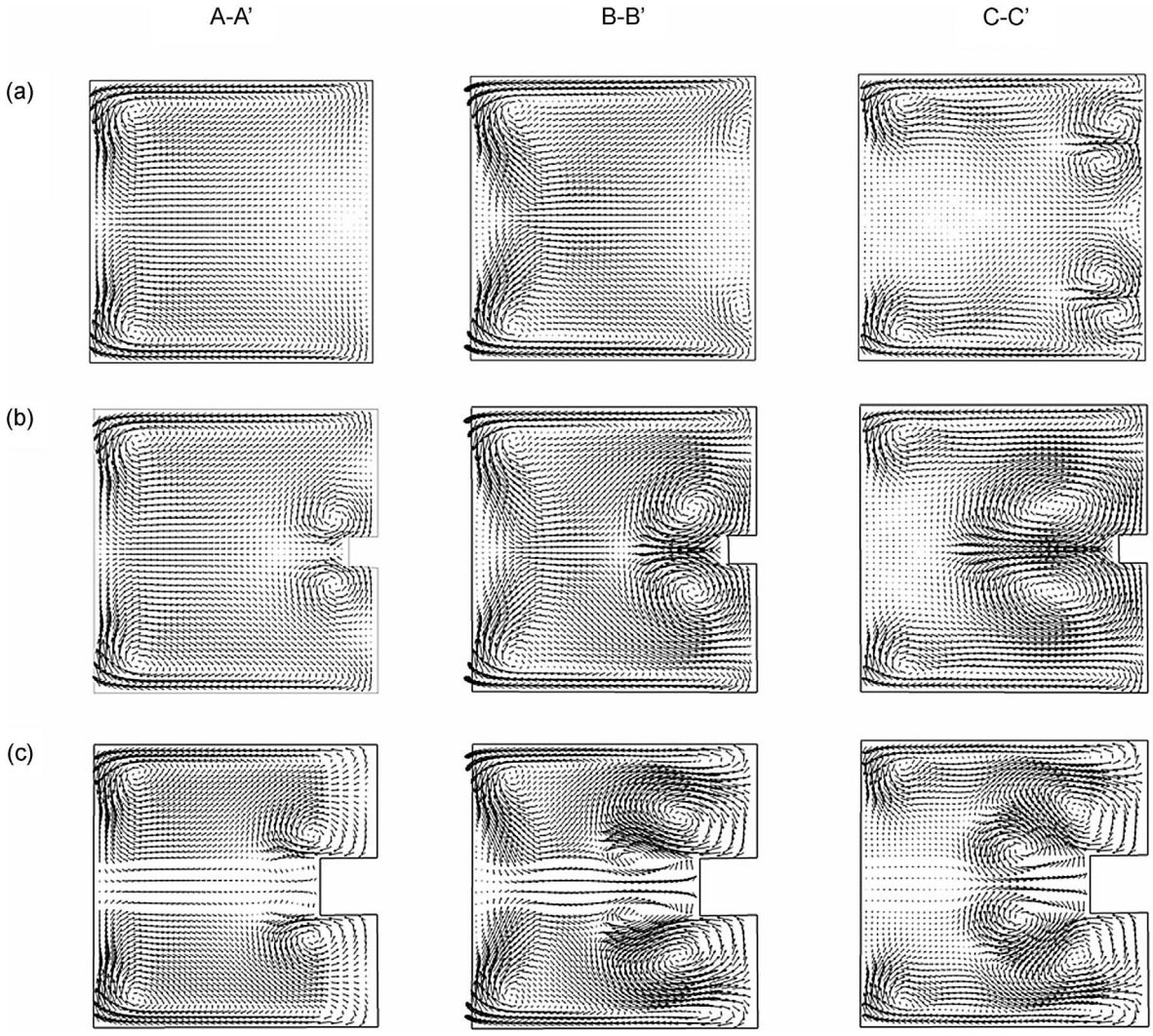

Fig. 2. Flow analysis: secondary flow motions on cross-sectional planes at A–A′, B–B′ and C–C′. (a) No rib; (b) $h/d_{\mathrm{e}} = 1/10$; (c) $h/d_{\mathrm{e}} = 1/5$. On each cross-sectional plane, outer wall is at right-hand side, inner wall is at left-hand side.

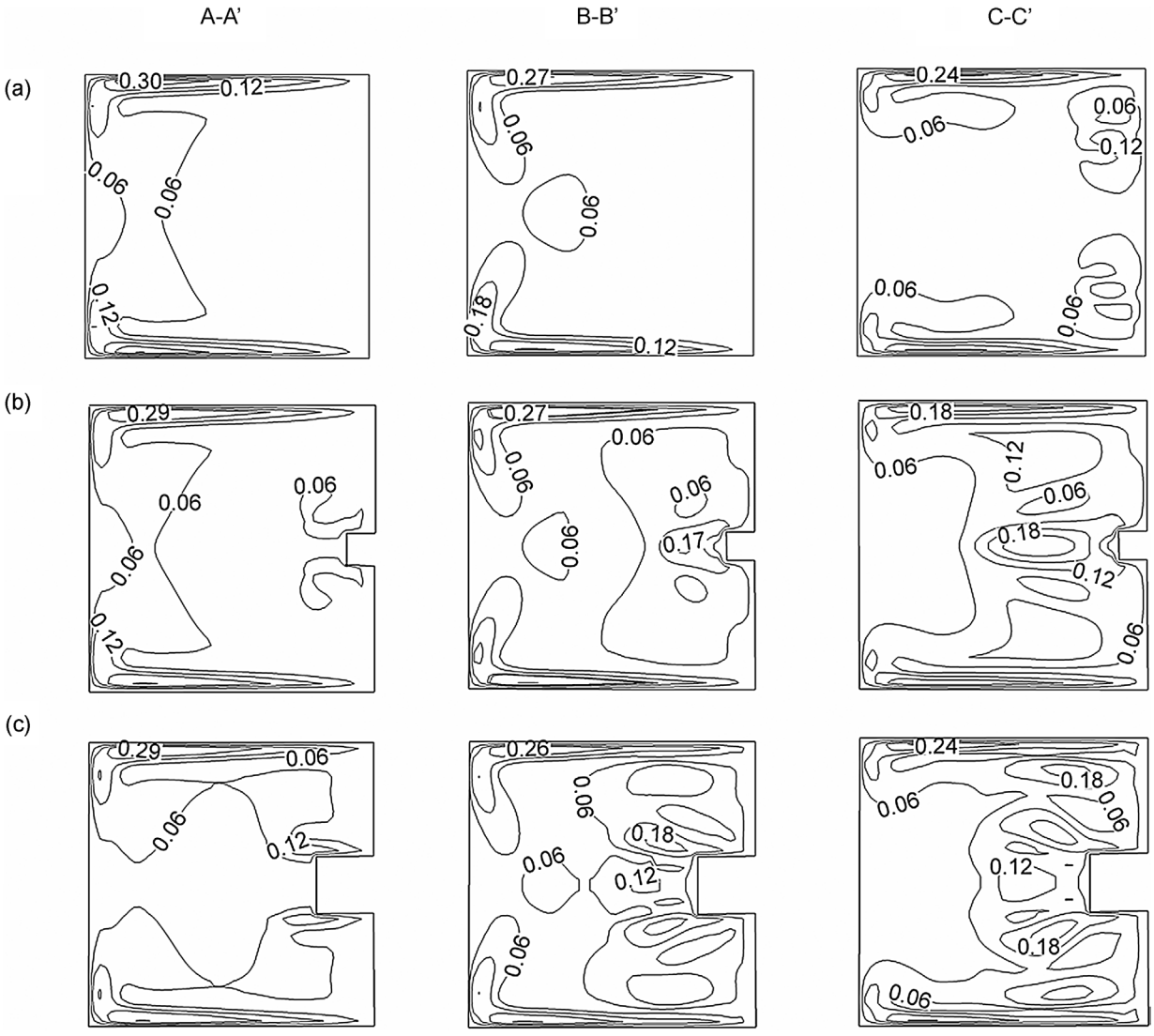

Fig. 3. Distributions of secondary kinetic energy coefficient, C_{sec}, on cross-sectional planes at A–A′, B–B′ and C–C′. (a) No rib; (b) $h/d_{\mathrm{e}} = 1/10$; (c) $h/d_{\mathrm{e}} = 1/5$. On each cross-sectional plane, outer wall is at right-hand side, inner wall is at left-hand side.

3.2. Numerical method

All the above-mentioned equations accompanied by boundary conditions are discretized using finite volume formulation. In the equations, the convective terms are modeled by the secondary-order upwind scheme while the diffusive terms are modeled by the central difference scheme. The numerical solution procedure adopts the well-known semi-implicit SIMPLE algorithm, which was developed by Launder and Spalding [20]. The detailed numerical procedure is given in the book of Patankar [21]. The convergent criterion is set as the relative residual of all variables, including the mass, all velocity components and temperature less than 10^{-4}. The results have been compared with those from the calculation with the convergent criterion set as 10^{-6}. The results are almost the same. A commercial CFD software CFD RC (ESI US R&D, Inc.) is used for the numerical solutions.

4. Results and discussion

The accuracy of numerical solutions has been investigated through the comparison of numerical results with experimental data in the curved duct with various aspect ratios in the previous study of Ko and Ting [18]. From the comparisons, the accuracy of numerical results has been verified. The grid independent tests were also carried out in the study of Ko and Ting [18]. For higher resolution of the current problem, the grid number is raised to 202 500 for ducts with various rib sizes. The grid layout is 45×45 on the rectangular cross-sectional plane, and 100 grids along the axial direction.

In the following, the flow fields, including the secondary vortices, distributions of velocity, temperature, and entropy generation, under a baseline flow condition, $q^* = 0.112$ and $De = 2000$, is first discussed, and then the effects q^* and De on the entropy generation is presented. From the inves-

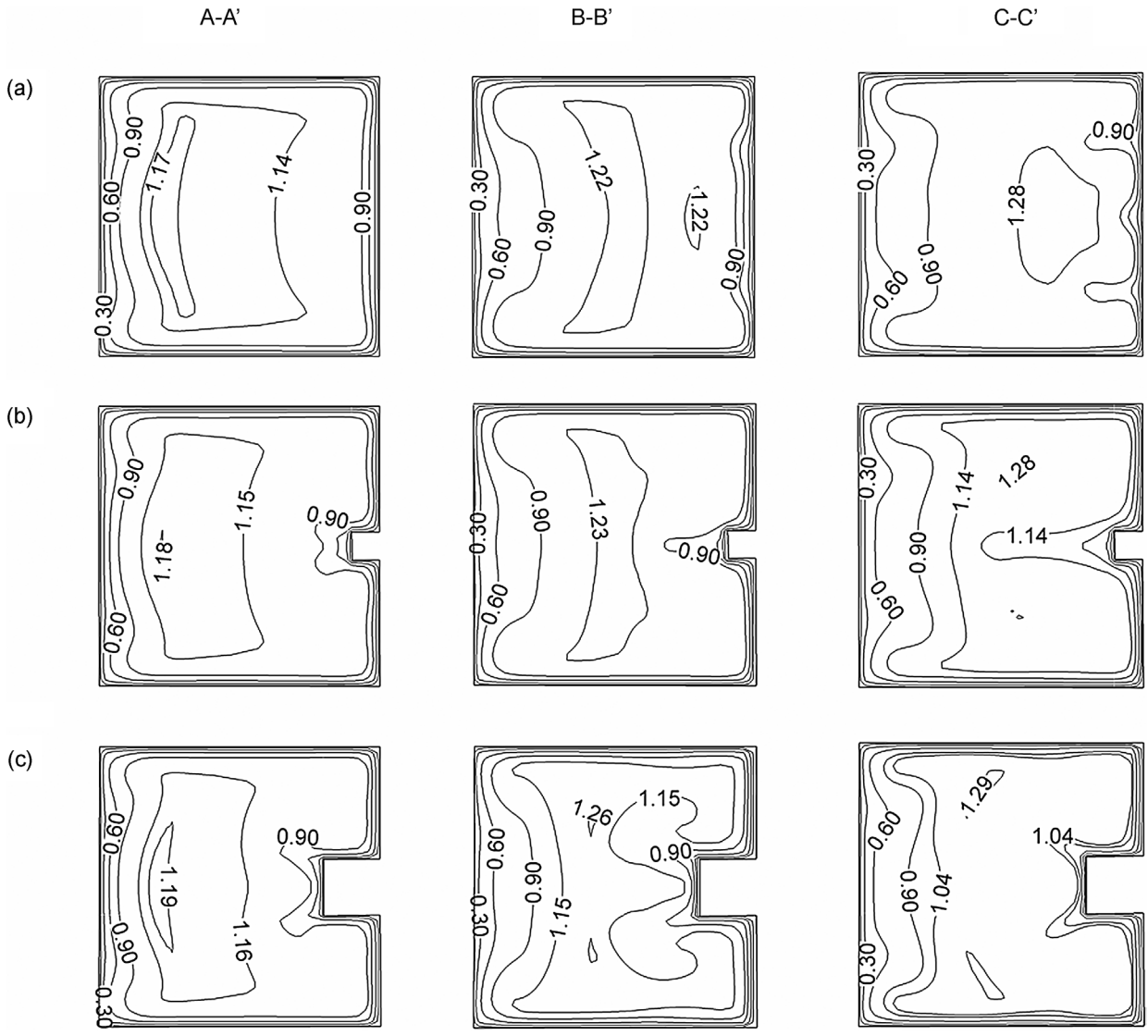

Fig. 4. Flow analysis: velocity contours on cross-sectional planes at A–A′, B–B′ and C–C′. (a) No rib; (b) $h/d_e = 1/10$; (c) $h/d_e = 1/5$. On each cross-sectional plane, outer wall is at right-hand side, inner wall is at left-hand side.

tigations of influences of ribs, the optimal rib size for the curved duct flow under various external heat flux and *De* is discussed.

4.1. Analysis of flow fields with $q^* = 0.112$ and $De = 2000$

The flow fields with flow conditions as $q^* = 0.112$ and $De = 2000$ will be discussed first. The case without rib and the ribbed cases with $h/d_e = 1/10$ and $1/5$ are selected as baseline cases for comparisons. Figs. 2(a)–(c) show the secondary vortices on the cross-sectional plane A–A′, B–B′ and C–C′ for the case without rib, and the ribbed cases with $h/d_e = 1/10$ and $1/5$, respectively. In the figures, the left-hand side of the cross-sectional plane is the inner wall of the curved duct, and the right side is the outer wall of the curved duct, which is exposed to the external heat flux. For the case without rib, as shown in Fig. 2(a), it can be found a pair of counter-rotating vortices distribute on the two corner regions near the inner wall on A–A′ plane. As the flow develops to B–B′ plane, the pair of vortices remain at nearly the same location. Meanwhile, two additional vortices with opposite rotating direction appear in the corner region near the outer wall. Further to C–C′ plane, the pair of vortices near the outer wall splits into two vortex pairs, and a vortex system with totally three pairs of vortices form on the plane. The complicated development of the secondary vortices is the result of combined effects of duct curvature and the centrifugal forces. Figs. 2(b) and 2(c) show the secondary vortices on the curved duct with rib of $h/d_e = 1/10$ and $1/5$, respectively. On all the three cross-sectional planes, it can be seen that the influence of rib on the vortices at the corners near inner wall is relatively minor, whereas the principal influences of ribs on the secondary vortices appear in the region near the outer wall. In both ribbed cases, a new pair of counter-rotating vortices forms near the rib corner on A–A′ plane.

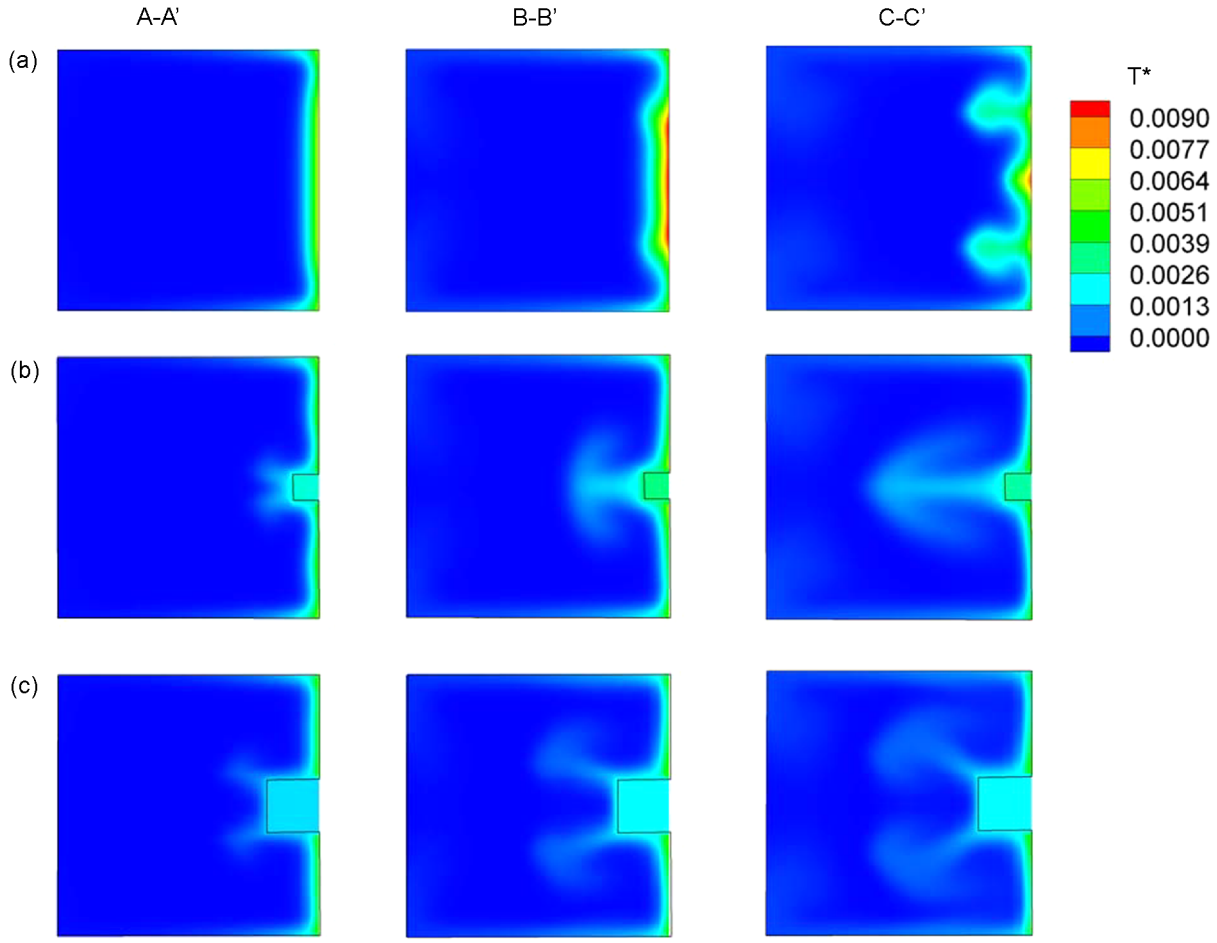

Fig. 5. Flow analysis: temperature contours on cross-sectional planes at A–A′, B–B′ and C–C′. (a) No rib; (b) $h/d_e = 1/10$; (c) $h/d_e = 1/5$. On each cross-sectional plane, outer wall is at right-hand side, inner wall is at left-hand side.

As the flow develops to B–B′ plane, the new vortex pair becomes stronger and moves their position slightly away from the rib corners in the case with rib of $h/d_e = 1/10$. Nonetheless, the principal vortex pattern remains unchanged near the rib corners in the case. As the rib size increases to $h/d_e = 1/5$, the vortex system near the rib becomes very complicated. On B–B′ plane, the vortex pair appearing near the rib corner on the A–A′ plane still distributes there. But between the vortex couple, a new pair of vortices develops and forms in the left region adjacent to the rib. As the flow develops to C–C′ plane, the three pairs of vortices become more distinguishable. The vortex system on the three cross-sectional planes for the three cases with or without ribs can be seen very different, which indicates the rib has significant influences on the secondary flow motion in the curved duct. Such influences will be beneficial to the enhancement of heat transfer performance but detrimental to the reduction of fluid friction in flow fields. Figs. 3(a)–(c) show the distributions of secondary kinetic energy coefficient, C_{sec}, which is defined as

$$C_{sec} = \left(V_1^2 + W_1^2\right)^{1/2} / V \tag{14}$$

where V_1 and W_1 are two velocity components on the corresponding cross-sectional planes. From the figures, the larger C_{sec} concentrates in a very narrow region near the top and bottom walls for all of the three cases. Although the value of the largest value of C_{sec} for the three cases is similar, which is around 0.29–0.3, the area coverage with larger C_{sec} becomes wider as the rib added and the rib size increases. Accordingly, the addition of rib can be seen to augment the secondary vortex motion. Figs. 4(a)–(c) show the velocity contours on the three cross-sectional planes for the three cases. For the case without rib, it can be seen clearly that the high velocity zone transfers from the inner side gradually toward the outer side as the flow develops from A–A′ plane to C–C′ plane. Such change is resulted from the influence of centrifugal force. However, the trend is changed due to the rib. From the ribbed cases, as shown in Figs. 4(b) and 4(c), the transfer of the high velocity zone is impeded by the rib, which results that the high velocity zone distributes near the central zone instead of outer zone of the cross-sectional duct plane as the flow develops toward downstream. In addition, the impediment effect of the rib can be seen to increase as the rib size increases.

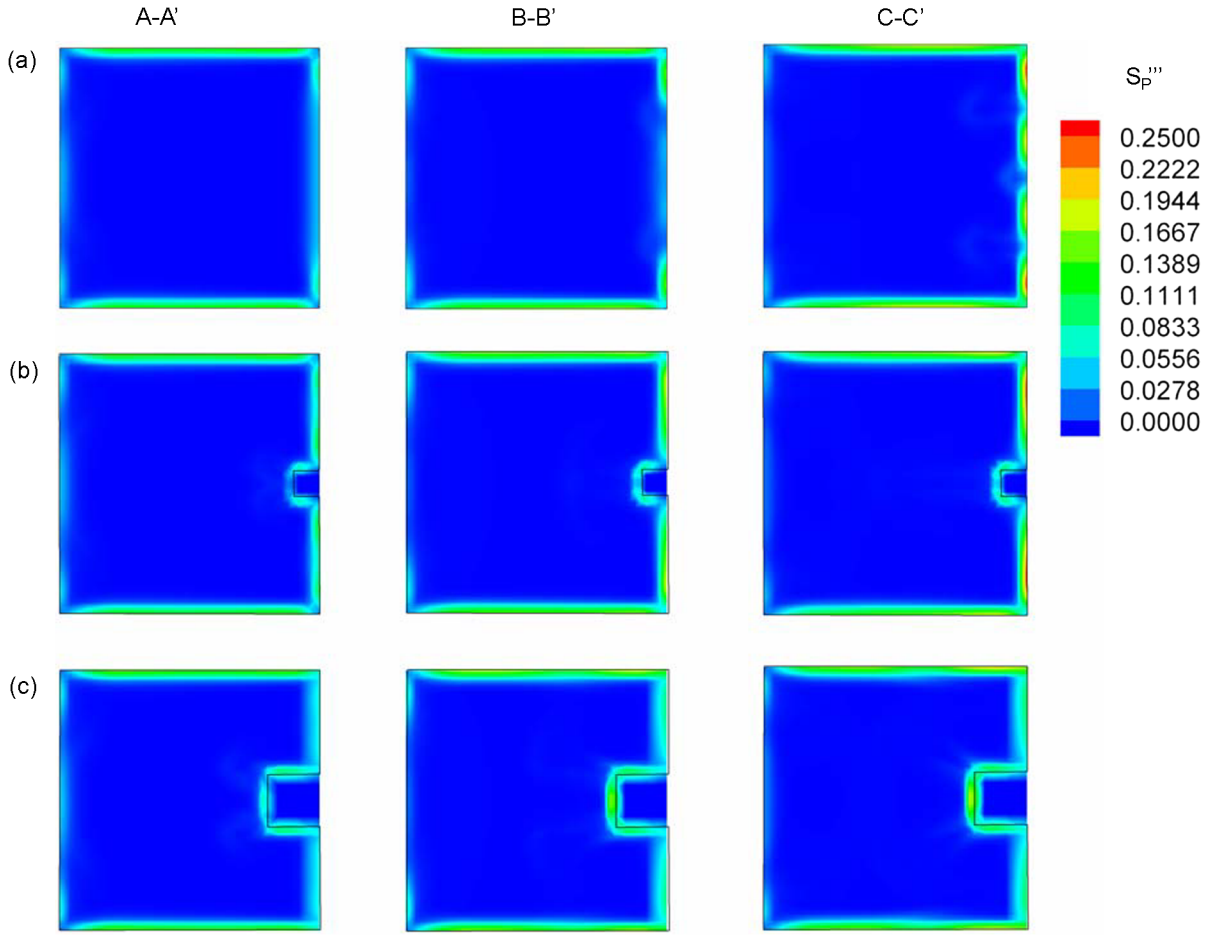

Fig. 6. The contours of volumetric entropy generation, S_P''', on cross-sectional planes at A–A′, B–B′ and C–C′. (a) No rib; (b) $h/d_e = 1/10$; (c) $h/d_e = 1/5$. On each cross-sectional plane, outer wall is at right-hand side, inner wall is at left-hand side.

Figs. 5(a)–(c) show the non-dimensional temperature contours on the three cross-sectional planes for the three cases, respectively. The non-dimensional temperature, T^*, is defined as

$$T^* = (T - T_0)/T_0 \tag{15}$$

Obviously, the principal temperature rise occurs in a very narrow region close to the outer wall, which is exposed to the external heat flux. The largest T^* is about 0.009 occurring in the case without rib. Besides, the temperature gradient can be found more serious in the case without rib. In the regions near the outer wall, the higher-temperature zones show different shapes on various cross-sectional planes for different cases. However, it is interesting to find that the shapes of the higher-temperature zones are coincident with the contours of relatively lower velocity near the outer wall as shown in Fig. 4. The results indicate the heat transfer performance is relatively worse in the lower-velocity region near the heated wall; therefore, the local temperature is higher. In the ribbed cases, it can be seen the temperature distribution within the rib is very uniform, which could be understood because of the large thermal conductivity of the rib. In addition, the temperature within the rib decreases as the rib size increases. These results reveal that the rib can effectively enhance the heat transfer performance in the curved duct, and in turn smooth the temperature gradient in flow fields.

4.2. *Analysis of entropy generation under flow condition of* $q^* = 0.112$ *and* $De = 2000$

The distributions of volumetric entropy generation due to frictional irreversibility and heat transfer irreversibility for the case without rib and the ribbed cases with $h/d_e = 1/10$ and $1/5$ under flow condition of $q^* = 0.112$ and $De = 2000$ are shown in Figs. 6 and 7, respectively. From Figs. 6(a)–(c), which show the distributions of S_P''' on the three cross-sectional planes, respectively, the significant entropy generation due to fluid frictional irreversibility is found to concentrate in a very thin layer adjacent to the curved duct wall. In all of the three cases, the values of S_P''' near the inner wall are relatively smaller than those near the other three sides. Although the largest S_P''' occurs in the regions closely adjacent to the outer wall in the case without rib, the distributing area of the layer with significant values of S_P''' can be seen to increase with the rib size. This is resulted from the more serious fluid friction near the wider rib-wall area in the larger

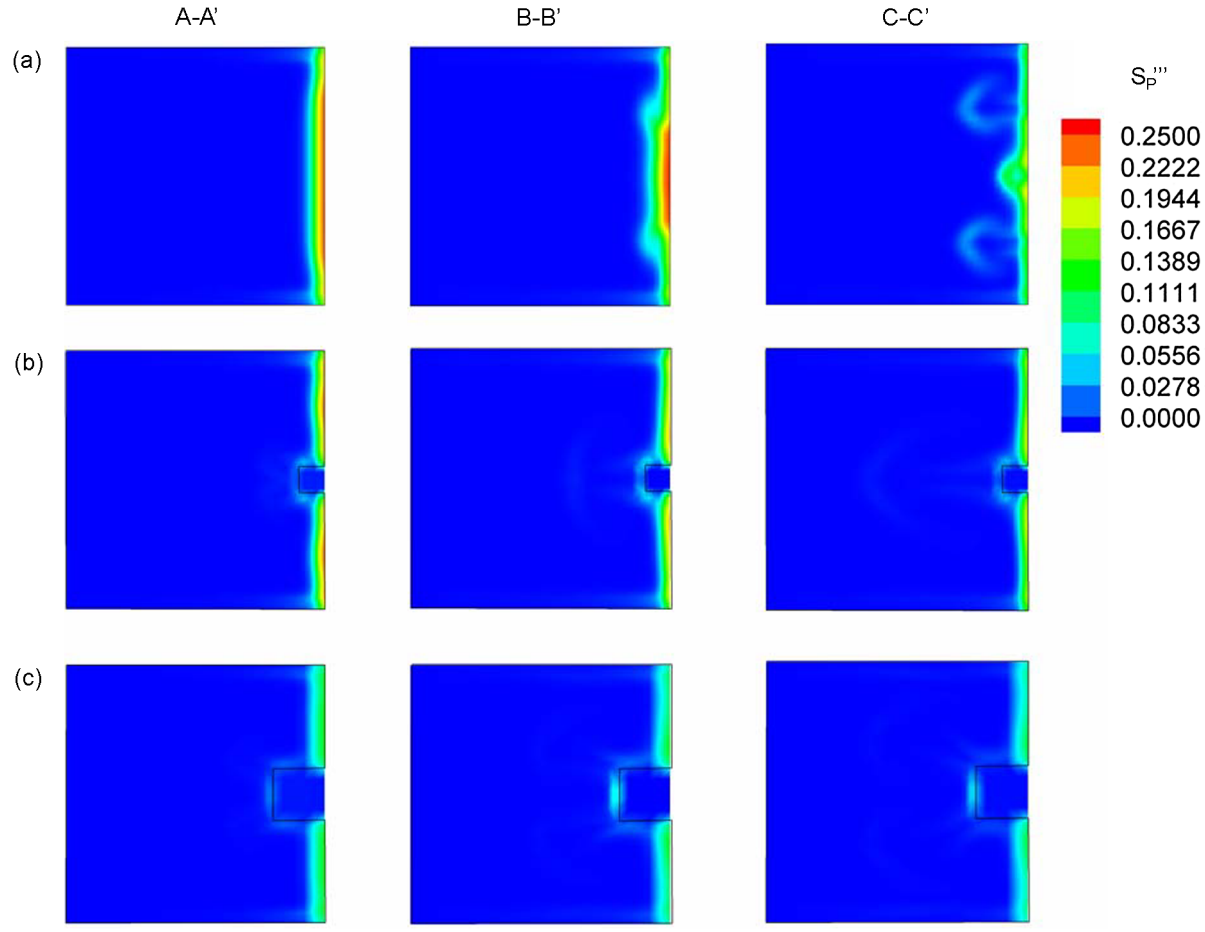

Fig. 7. The contours of volumetric entropy generation, S_T''', on cross-sectional planes at A–A′, B–B′ and C–C′. (a) No rib; (b) $h/d_e = 1/10$; (c) $h/d_e = 1/5$. On each cross-sectional plane, outer wall is at right-hand side, inner wall is at left-hand side.

rib case. The distributions of S_T''' on the three cross-sectional planes for the three cases are shown in Figs. 7(a)–(c), respectively. The distribution of significant S_T''' only occurs in the region close to the outer wall, whereas S_T''' is almost zero in other regions. The largest S_T''' occurs in the case without rib. Both of the magnitude and distributing zone of significant S_T''' can be seen to be smaller in the ribbed cases. As the rib size increases, S_T''' decreases obviously. These results verify again that the rib can effectively enhance the heat transfer performance, reduce the temperature gradient, and accordingly decrease the entropy generation due to heat transfer irreversibility. The contours of *Be* on the three cross-sectional planes for the three cases are shown in Fig. 8. From the figure, it can be found that the values of *Be* near the outer wall are larger than 0.5, which indicates S_T''' is larger than S_P''' in the region where the external heat flux is imposed. The area of fluid flow region with larger *Be* can be seen to become smaller in the two ribbed cases. Besides, as rib size increases from $h/d_e = 1/10$ to $1/5$, the values of *Be* can be seen to become smaller in most region of the flow field, which reveals that S_T''' decreases as the rib size increases. The distribution of S_{gen}''' on the three cross-sectional planes for the three cases is shown in Fig. 9, from which it can be seen that the significant S_{gen}''' concentrates only in the thin layer on the perimeter of the duct wall for all the three cases. The value of S_{gen}''' is largest in the region near the outer wall, whereas S_{gen}''' is very minor in the region near the inner wall.

4.3. Effects of rib size on entropy generation and analysis of optimal rib size

For evaluation of the entropy generation in flow fields, the non-dimensional entropy generation rate, S_P^*, S_T^* and S_{gen}^*, in the whole curved duct are defined by

$$S_P^* = \frac{\int_V S_P'''\,dV}{\dot{Q}/T_0} \tag{16}$$

$$S_T^* = \frac{\int_V S_T'''\,dV}{\dot{Q}/T_0} \tag{17}$$

and

$$S_{gen}^* = \frac{\int_V S_{gen}'''\,dV}{\dot{Q}/T_0} \tag{18}$$

where V is the volume of the whole computational domain, including the fluid and the steel rib; $\dot{Q}$ is the heat flow rate into the flow field. The comparison of entropy generation

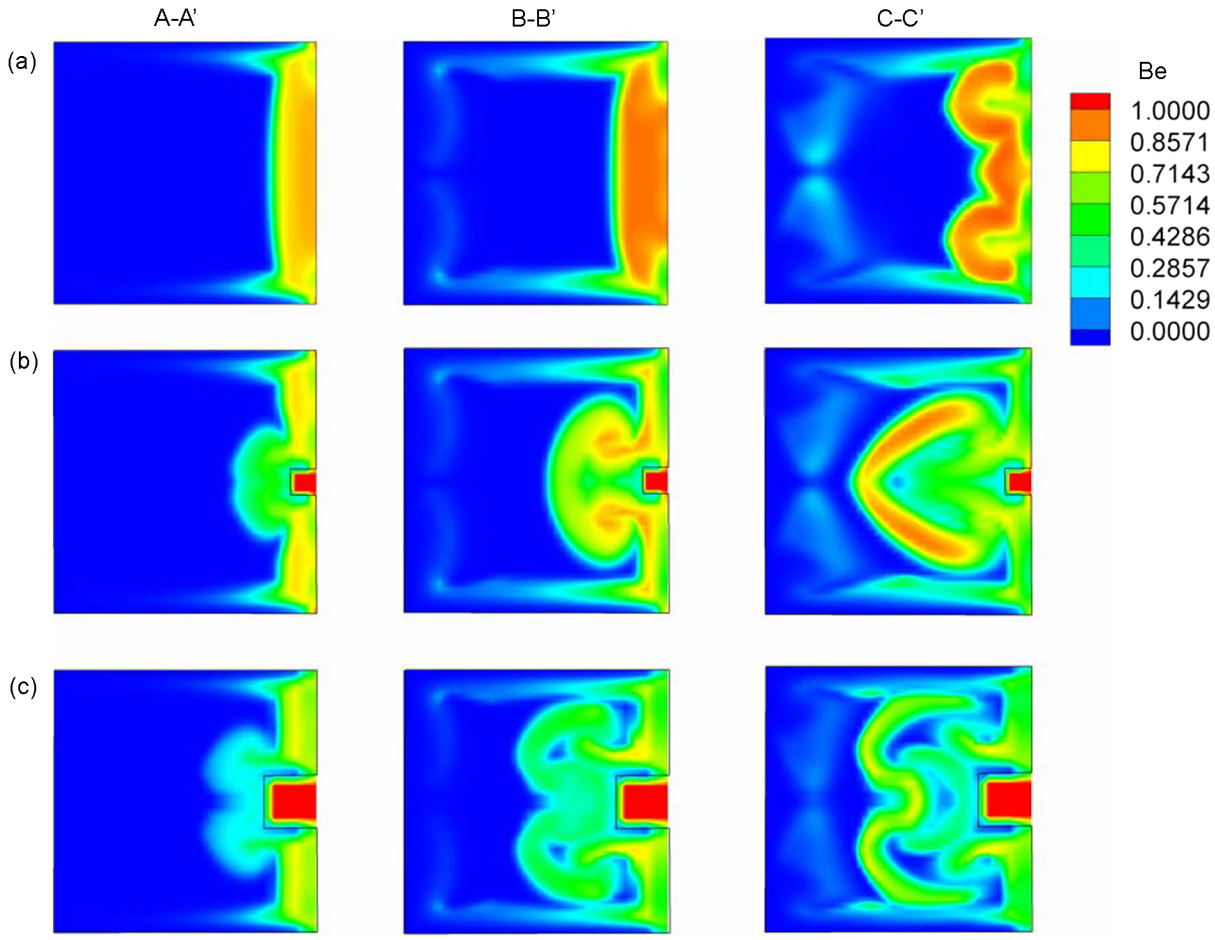

Fig. 8. The contours of *Be* on cross-sectional planes at A–A′, B–B′ and C–C′. (a) No rib; (b) $h/d_e = 1/10$; (c) $h/d_e = 1/5$. On each cross-sectional plane, outer wall is at right-hand side, inner wall is at left-hand side.

for the cases without rib and the ribbed cases with different rib sizes, including $h/d_e = 1/10, 1/7$ and $1/5$, is shown in Fig. 10. A clear trend can be found from the figure that S_P^* in all ribbed cases is larger than that in the case without rib, and its magnitude increases as the rib size increases. The results can be understood as a consequence that more fluid friction is induced by the wider rib wall in the larger rib case. The figure also indicates that the rib can cause obvious reduction of S_T^*. As the rib size becomes larger, S_T^* decreases more, which reveal again that the effect of the rib on heat transfer performance is substantial. For the present analyzed case with $q^* = 0.112$ and $De = 2000$, S_P^* is much larger than S_T^* for all the cases, indicating the entropy generation under the current flow condition is dominated by the fluid frictional irreversibility. It is noted that Fig. 10 also exhibits the opposite influence of rib size on S_P^* and S_T^*. The conflict trend manifests that the rib size could be optimized due to a trade-off between the irreversibility from heat transfer and fluid friction so that the minimal resultant entropy generation could be obtained. From Fig. 11, which depicts the values of S_T^*/S_{gen}^* for all the different cases, it can be seen that the values of S_T^*/S_{gen}^* for all cases is less than 0.5. In addition, the value of S_T^*/S_{gen}^* decreases as the rib size increases, which points out that the entropy generation due to fluid frictional irreversibility in the whole flow field becomes increasingly more important than that from heat transfer irreversibility as the rib size increases. The resultant entropy generation S_{gen}^* for the calculated cases is depicted in Fig. 12. It can be found that the S_{gen}^* can be effectively reduced by adding ribs with all sizes considered in the present study. Nonetheless, among the analyzed ribbed cases, the rib size of $h/d_e = 1/7$ can induce the minimal S_{gen}^*. Accordingly, the rib size is concluded as the optimal option for the curved duct under the flow condition with $q^* = 0.112$ and $De = 2000$. By equipped the rib of such size, the best exergy utilization with least irreversibility could be obtained in the convective flow of the curved duct.

4.4. Effects of Dean number and external heat flux

For further investigating the entropy generation and optimal rib size under different flow conditions, several cases with various q^* and *De* are calculated. Figs. 13(a) and 13(b) show the values of S_P^* and S_T^* for $q^* = 0.112$ cases with $De = 500$, 1000, 2000 and 3000, respectively. Comparing the two figures, it can be seen that the increase of *De* makes

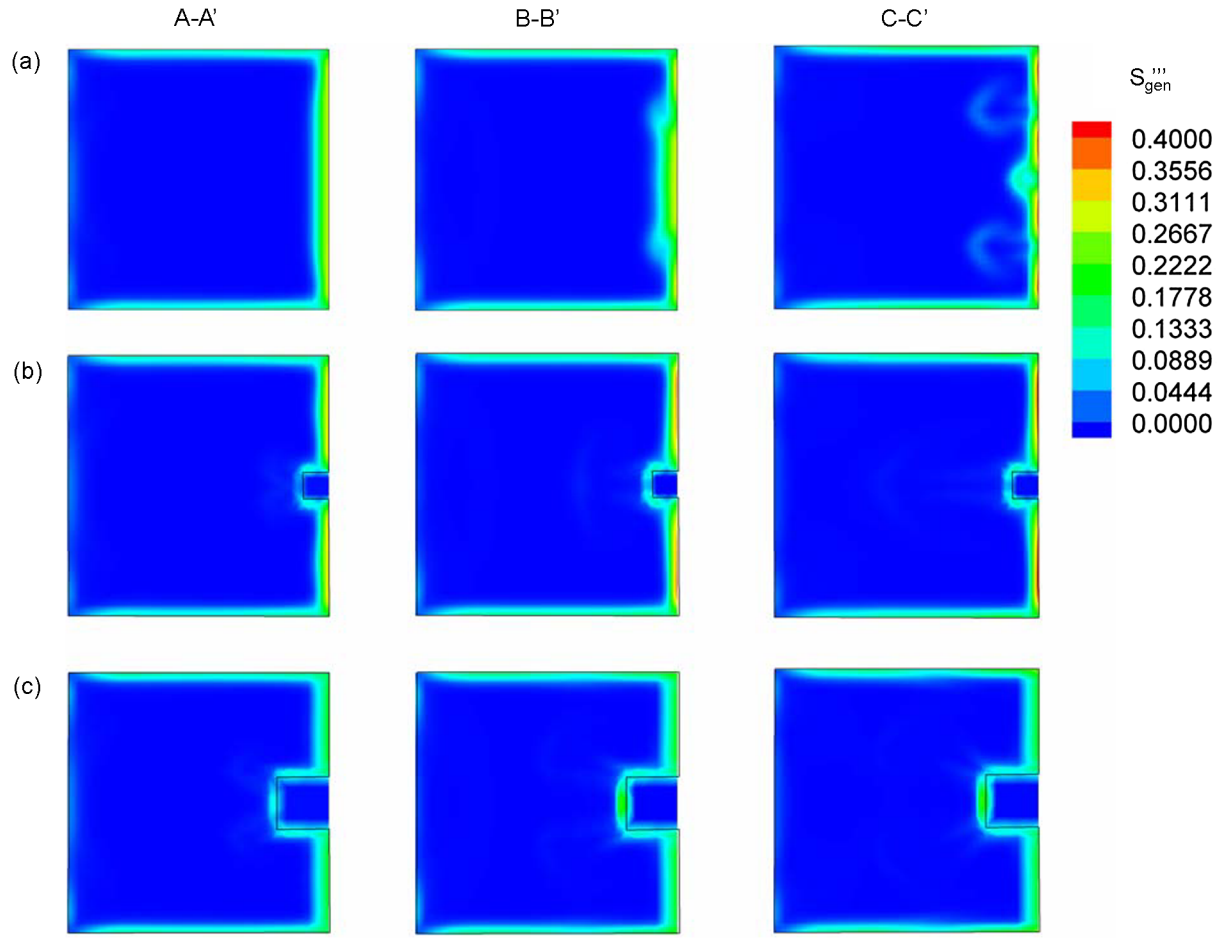

Fig. 9. The contours of volumetric entropy generation, S'''_{gen}, on cross-sectional planes at A–A′, B–B′ and C–C′. (a) No rib; (b) $h/d_e = 1/10$; (c) $h/d_e = 1/5$. On each cross-sectional plane, outer wall is at right-hand side, inner wall is at left-hand side.

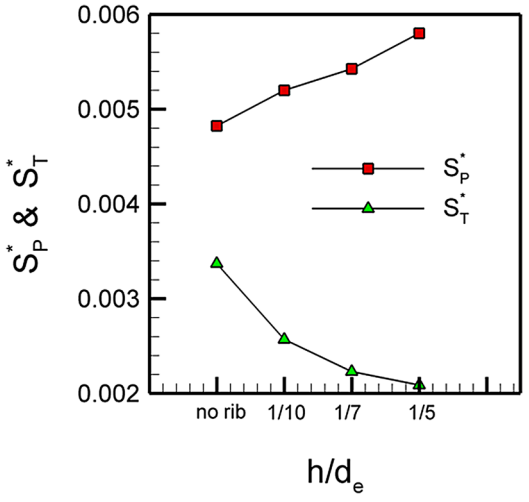

Fig. 10. The effects of rib height on entropy generation induced from heat transfer (S^*_T) and fluid friction (S^*_P).

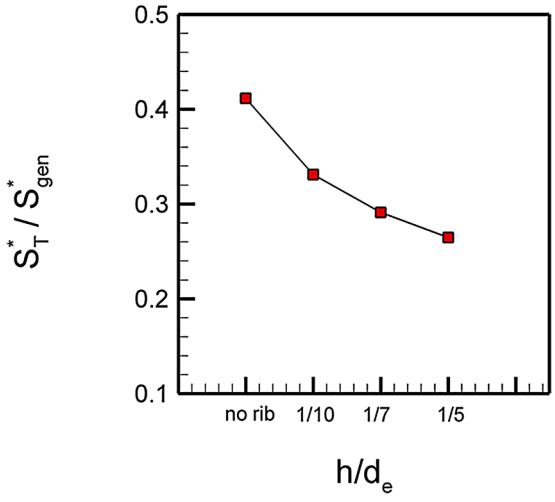

Fig. 11. The effects of rib height on S^*_T/S^*_{gen}.

S^*_P increase and S^*_T decrease. Such results can be understood that the increase of *De* will cause the more serious fluid friction and the better heat transfer performance. For the same reasons, S^*_P increases and S^*_T decreases as the rib is added and the rib size becomes larger. Fig. 14 shows the values of S^*_T/S^*_{gen} for $q^* = 0.112$ cases with $De = 500$, 1000, 2000 and 3000, respectively. It can be seen from the figure that the value of S^*_T/S^*_{gen} gradually decreases as the rib size increases for all *De* cases, which indicates the trend that the

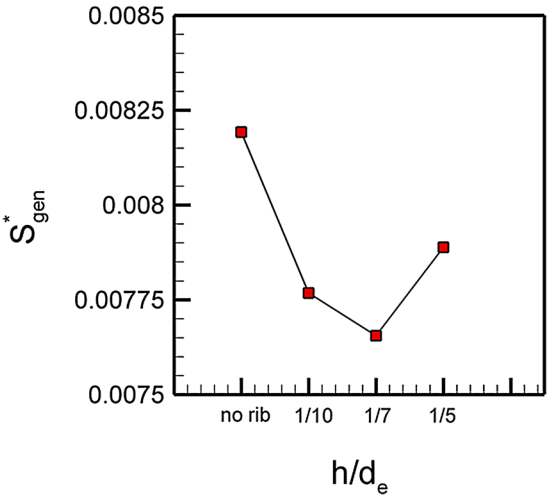

Fig. 12. The effects of rib height on entropy generation, S^*_{gen}.

rib can enhance the heat transfer performance and in turn to reduce heat transfer irreversibility is not influenced by *De*. As the rib size increases, the affects can be found to become more significant. The figure also exhibits that the value of S^*_T/S^*_{gen} becomes larger as *De* becomes smaller. In all ribbed and non-ribbed cases with $De = 500$ and 1000, S^*_T/S^*_{gen} is much larger than 0.5, whereas S^*_T/S^*_{gen} is less than 0.5 for all cases as *De* increases to 2000. As *De* increases to 3000, the values of S^*_T/S^*_{gen} in all cases become much smaller than 0.5. This reveals the fact that the entropy generation in flow fields is more dominant by heat transfer irreversibility in smaller *De* cases, and is more dominant by frictional irreversibility when *De* is larger. The increase of S^*_P and decrease of S^*_T caused by the increase of *De* accordingly induces the decrease of S^*_T/S^*_{gen}. The effects of *De* on S^*_{gen} are shown in Fig. 15. In $De = 2000$ cases, which has been discussed previously, the magnitude of S^*_{gen} can be reduced by adding the rib in the curved duct, and the optimal rib size is $h/d_e = 1/7$. The similarly favorable effect of the added rib can also be found in $De = 500$ and 1000 cases. As the rib is added, the value of S^*_{gen} decreases monotonically as the rib size increases, which results that $h/d_e = 1/5$ is the optimal rib size for the $De = 500$ and 1000 cases. However, when *De* increases to 3000, the opposite and unexpected results are found from the figure. In $De = 3000$ cases, the added rib does not reduce the value of S^*_{gen} but makes the value increase. As the rib size becomes larger, the entropy generation becomes more serious. These results point out that the rib should not be added in the curved duct from the view point of minimal entropy principle when *De* is larger. The reasons to cause such results can be explained as follows. Although the addition of rib can reduce S^*_T through the enhancement of heat transfer performance, but it also raises S^*_P simultaneously because the added rib makes fluid friction become more serious in flow fields. Since the entropy generation is dominated by frictional irreversibility in the larger *De* ($De = 3000$) cases, as been discussed previously, the increase of S^*_P overwhelms the decrease of S^*_T; therefore the

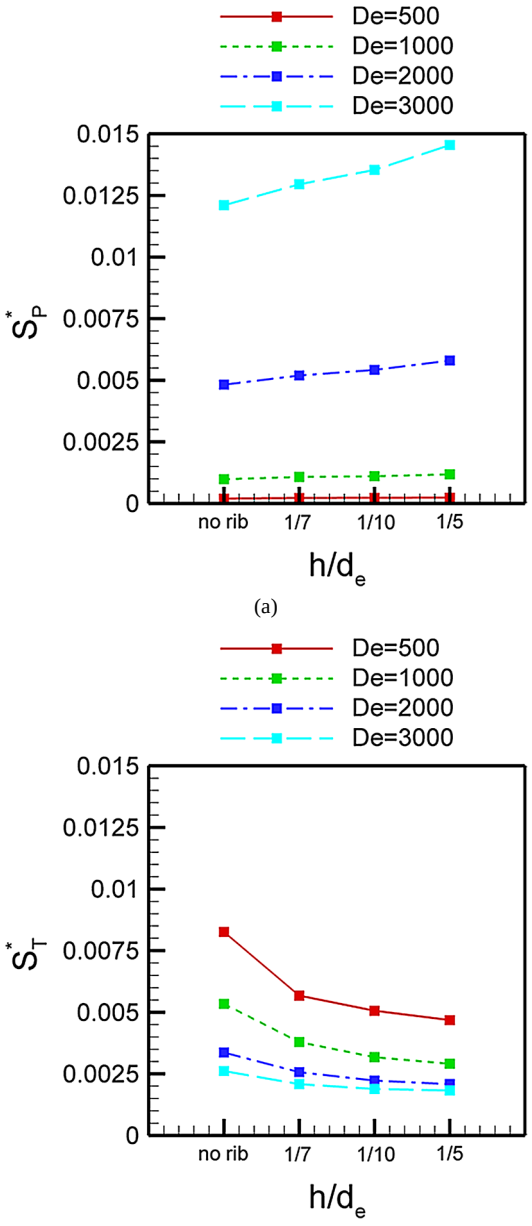

Fig. 13. (a) Effects of *De* on S^*_P ($q^* = 0.112$). (b) Effects of *De* on S^*_T ($q^* = 0.112$).

addition of ribs induces the unexpected increase of resultant S^*_{gen}. As the rib size increases, the unexpected increase of resultant S^*_{gen} becomes larger. On the contrary, the entropy generation is dominated by heat transfer irreversibility in the smaller *De* cases ($De = 500$ and 1000), the addition of rib can effectively reduce S^*_T. Although the S^*_P increases due to the added rib at the same time, the resultant entropy generation S^*_{gen} still decreases since the dominant entropy generation is S^*_T for the smaller *De* cases. The affects also become more significant as rib size increases. Accordingly, in $De = 500$ and 1000 cases S^*_{gen} can be reduced by adding ribs of all sizes, and the optimal rib size is $h/d_e = 1/5$, which is the largest rib size considered in present study. As for the

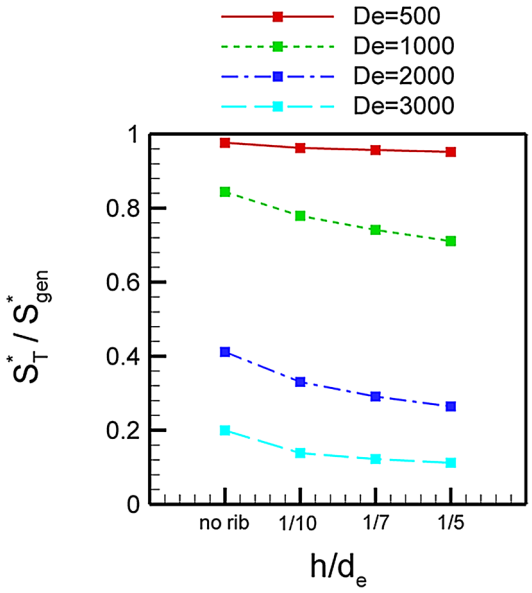

Fig. 14. Effects of De on S^*_T/S^*_{gen} ($q^* = 0.112$).

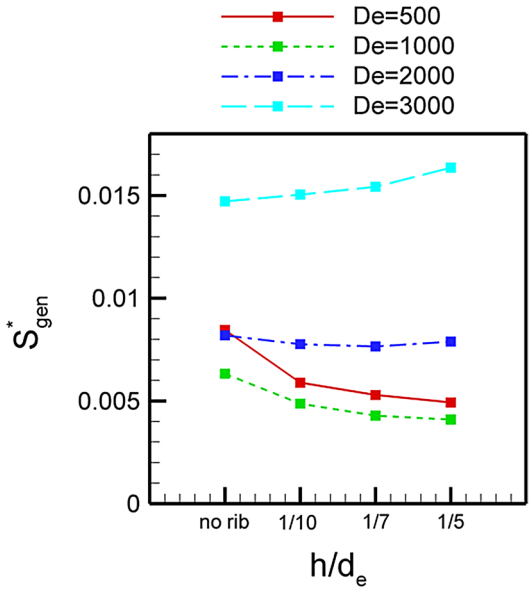

Fig. 15. Effects of De on S^*_{gen} ($De = 2000$).

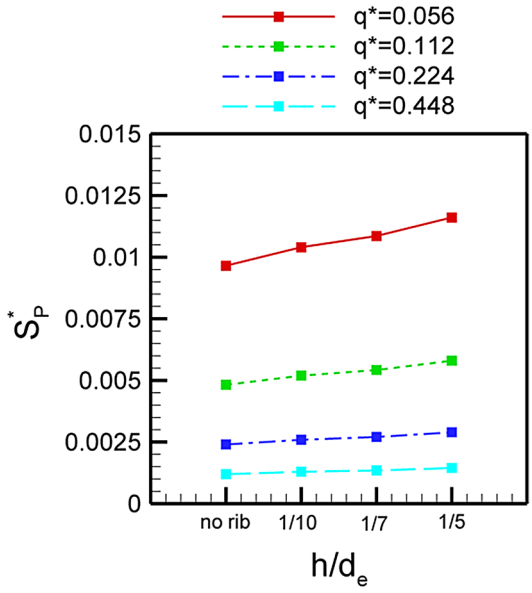

(a)

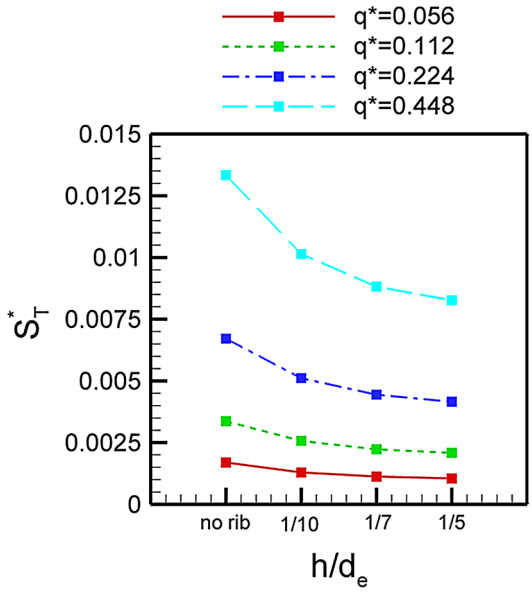

(b)

Fig. 16. (a) Effects of q^* on S^*_P ($De = 2000$). (b) Effects of q^* on S^*_T ($De = 2000$).

$De = 2000$ cases, the entropy generation due to frictional and heat transfer irreversibility is relatively comparable, i.e. no one is dominant in flow fields. Therefore, the opposite influence of added rib on S^*_P and S^*_T makes the choice of optimal trade-off of the rib size become necessary to obtain the minimal S^*_{gen}. The details have been discussed previously.

The effects of the external heat flux are shown in Figs. 16–17. In the calculated cases, De is fixed as 2000, and q^* is varied as 0.056, 0.112, 0.224 and 0.448, respectively. Figs. 16(a) and 16(b) show the values of S^*_P and S^*_T for $De = 2000$ cases with $q^* = 0.056$, 0.112, 0.224 and 0.448, respectively. From the two figures, it can be seen that the increase of q^* makes S^*_P decrease and S^*_T increase. The increase of S^*_T is resulted from the more serious heat transfer irreversibility in larger q^* cases. Because the temperature raise is limited for the heat flux considered in the present study, the influence of heat flux on velocity fields is minor. Therefore, S'''_P, which is mainly related with the velocity gradient, is not significantly affected by heat flux. However, due to the normalization of $\dot{Q}/T_0$ and temperature term appears in the dominator of the definition of S^*_P (see Eq. (16)), S^*_P is induced to become larger in the smaller q^* cases. The effects of rib on S^*_P and S^*_T remain the same for all heat flux cases, i.e. the added rib causes S^*_P to increase whilst causes S^*_T to decrease. The change increases as the rib size becomes larger. Fig. 17 shows the values of S^*_T/S^*_{gen} for these cases, from which it can be seen that S^*_T/S^*_{gen} increases as q^* in-

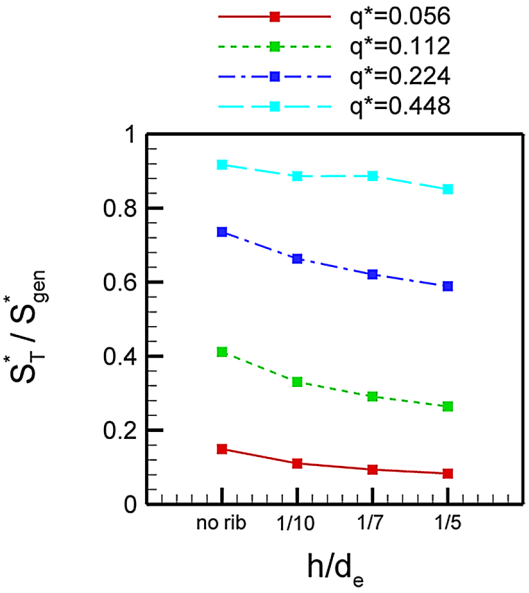

Fig. 17. Effects of q^* on S^*_T/S^*_{gen} ($De = 2000$).

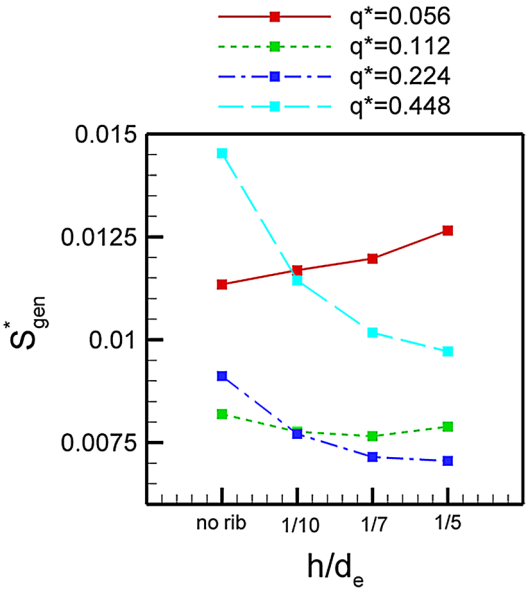

Fig. 18. Effects of q^* on S^*_{gen} ($De = 2000$).

creases. This is the natural result due to the larger S^*_T caused by the larger q^*. In larger q^* cases, the entropy generation is more dominant by heat transfer irreversibility. It can also be seen from the figure that the values of S^*_T/S^*_{gen} decrease monotonically as the rib size increases in all q^* cases, which indicates again the larger rib is helpful for the better heat transfer performance and the reduction of S^*_T. The resultant entropy generation S^*_{gen} for the cases is shown in Fig. 18. In the cases with $q^* = 0.112$, the addition of rib with all sizes can reduce the value of S^*_{gen} and the optimal rib size to induce minimal S^*_{gen} is $h/d_e = 1/7$ as pointed out previously. As for q^* decreases to 0.056, the addition of rib with all sizes cannot reduce S^*_{gen} but raises its value since the entropy generation is dominated by the frictional irreversibility in the low heat flux cases. Accordingly, the rib should not be added in the cases. As the external heat flux increases to $q^* = 0.224$ and 0.448, the major entropy generation comes from the heat transfer irreversibility. It can be seen that the addition of rib can cause the reduction of the value of S^*_{gen}. Besides, as rib size increases, S^*_{gen} decreases more. Therefore, the minimal S^*_{gen} is obtained in the $h/d_e = 1/5$ case, which is the largest rib size in the present study.

5. Conclusions

Three-dimensional laminar forced convective flow and entropy generation in a 180-deg curved rectangular duct with longitudinal ribs equipped on the heated wall have been investigated by numerical methods. The effects of rib size under different flow conditions with various Dean number and external flux are particularly highlighted. The principal conclusions are as follows:

(1) The major entropy generation concentrates in the region adjacent to the solid walls since the velocity and temperature gradients are steepest there. Near the duct outer wall, where the external heat flux is imposed, the entropy generation is largest. The entropy generation near the inner duct walls is relatively mild.

(2) The addition of ribs can augment the secondary vortex motion in the curved duct, through which the heat transfer performance is enhanced, and therefore, the temperature gradient in flow fields becomes milder. In turn, the entropy generation from the heat transfer irreversibility is effectively reduced. Nonetheless, since the flow is disturbed significantly and the solid walls become wider in the fluid flow due to the added ribs, more serious fluid friction is resulted. As a consequence, the entropy generation from fictional irreversibility is raised by the ribs. The opposite influence on the entropy generation from irreversibilities makes the optimal trade-off analysis become necessary for obtaining the minimal resultant entropy generation.

(3) For cases with smaller Dean number and larger heat flux, the entropy generation in flow fields is dominated by heat transfer irreversibility. Therefore, the addition of rib can reduce the resultant entropy generation effectively since the reduction of the entropy generation from heat transfer irreversibility overwhelms the increase of the entropy generation from frictional irreversibility due to the rib. On the contrary, since the entropy generation is dominated by frictional irreversibility in cases with larger Dean number and smaller heat flux, the addition of the rib cannot reduce the resultant entropy generation but raises its value. Accordingly, the rib should not be added in curved duct in these cases. For the cases with medium Dean number and exter-

nal heat flux, the decrease of entropy generation from heat transfer due to the rib competes with the simultaneous increase of entropy generation from frictional irreversibility, which makes the optimal rib size exist. The optimal rib size should be adopted so that the best exergy utilization can be achieved in the thermal system. These results given in the present paper provide worthwhile information for considerations of adding ribs on a curved duct from view point of thermodynamic second law.

References

[1] H. Ito, Flow in curved pipes, JMSE Int. J. 30 (1987) 543–552.
[2] Z.F. Dong, M.A. Ebadian, Numerical analysis of laminar flow in curved elliptic ducts, J. Fluid Engrg. 113 (1991) 555–562.
[3] K.C. Cheng, J. Nakayama, M. Akiyama, Effect of finite and infinite aspect ratios on flow patterns in curved rectangular channels, in: Flow Visualisation, Tokyo, Japan, 1977, pp. 181–186.
[4] C.J. Bolinder, B. Sunden, Numerical prediction of laminar flow and forced convective heat transfer in a helical square duct with a finite pitch, Int. J. Heat Mass Transfer 39 (15) (1996) 3101–3115.
[5] L. Wang, Buoyancy-force-driven transition in flow structures and their effects on heat transfer in a rotating curved channel, Int. J. Heat Mass Transfer 40 (2) (1997) 220–235.
[6] R.J. Silva, R.M. Valle, M. Ziviani, Numerical hydrodynamic and thermal analysis of laminar flow in curved elliptic and rectangular ducts, Int. J. Therm. Sci. 38 (1999) 585–594.
[7] T.T. Chandratilleke, Secondary flow characteristics and convective heat transfer in a curved rectangular duct with external heating, in: Proc. of 5th World Conference on Experimental Heat Transfer, Fluid Mechanics and Thermodynamics [ExHFT-5], Thessaloniki, Greece, September 24–28, 2001.
[8] T.T. Chandratilleke, Nursubyakto, Numerical prediction of secondary flow and convective heat transfer in externally heated curved rectangular ducts, Int. J. Therm. Sci. 42 (2003) 187–198.
[9] C. Camci, D.H. Rizzo, Secondary flow and forced convection heat transfer near endwall boundary layer fences in a 90-deg turning duct, Int. J. Heat Mass Transfer 45 (2002) 831–843.
[10] A. Bejan, Entropy Generation Minimization, CRC Press, Boca Raton, FL, 1996.
[11] A. Bejan, Entropy Generation Through Heat and Fluid Flow, Wiley, New York, 1982.
[12] P.K. Nag, N. Kumar, Second law optimization of convection heat transfer through a duct with constant heat flux, Int. J. Energy Res. 13 (1989) 537–543.
[13] A.Z. Sahin, Irreversibilities in various duct geometries with constant wall heat flux and laminar flow, Energy 23 (6) (1998) 465–473.
[14] A.Z. Sahin, Thermodynamics of laminar viscous flow through a duct subjected to constant heat flux, Energy 21 (12) (1996) 1179–1187.
[15] S.Z. Shuja, Optimal fin geometry based on exergoeconomic analysis for a pin-fin array with application to electronics cooling, Exergy 2 (2002) 248–258.
[16] O.N. Sara, S. Yapici, M. Yilmaz, T. Pekdemir, Secondary law analysis of rectangular channels with square pin-fins, Int. Comm. Heat Mass Transfer 28 (5) (2001) 617–630.
[17] T.H. Ko, K. Ting, Entropy generation and thermodynamic optimization of fully developed laminar convection in a helical coil, Int. Commun. Heat Mass Transfer 32 (2005) 214–223.
[18] T.H. Ko, K. Ting, Entropy generation and optimal analysis for laminar forced convection in curved rectangular ducts: a numerical study, Int. J. Therm. Sci. 45 (2) (2006) 138–150.
[19] S. Paoletti, F. Rispoli, E. Sciubba, Calculation of exergetic losses in compact heat exchanger passages, ASME AES 10 (1989) 21–29.
[20] B.E. Launder, D.B. Spalding, The numerical computation of turbulent flows, Comput. Methods Appl. Mech. Engrg. 3 (1974) 269–289.
[21] S.V. Patankar, Numerical Heat Transfer and Fluid Flow, Hemisphere, Washington, DC, 1980.